The Astrophysical Journal, 594:592–604, 2003 September 1

ELEMENTAL FRACTIONATION IN SMALL SOLAR ENERGETIC PARTICLE EVENTS

P. L. Slocum,[1,2] E. C. Stone,[3] R. A. Leske,[3] E. R. Christian,[4] C. M. S. Cohen,[3] A. C. Cummings,[3] M. I. Desai,[5]
J. R. Dwyer,[6] G. M. Mason,[5] J. E. Mazur,[2] R. A. Mewaldt,[3]
T. T. von Rosenvinge,[4] and M. E. Wiedenbeck[1]

Received 2003 January 13; accepted 2003 May 5

ABSTRACT

Using the Solar Isotope Spectrometer on the *Advanced Composition Explorer* (*ACE*), we have measured the 11.0–21.8 MeV nucleon^{-1} heavy ($Z \geq 6$) element abundances of 39 small solar energetic particle (SEP) events that occurred between 1998 April 3 and 2002 February 26. Using He isotope data from the Ultra–Low-Energy Isotope Spectrometer on *ACE*, we have classified the events according to their 0.5–2.0 MeV nucleon^{-1} ^{3}He/^{4}He ratios. We find that their average heavy-element composition is similar to that of either large gradual events or ^{3}He-rich events, depending on their ^{3}He/^{4}He ratio. As seen in recent studies of small SEP events, we find that the heavy-element intensities relative to C increase with the ^{3}He/^{4}He ratios. The dependence of the heavy-element abundances on first ionization potential (FIP) has been derived, using a model consisting of a power law in Q/M (and Z) times a step function in FIP. We report the magnitude of the FIP factor in each event and find that it varies from ~2 to 7 with no clear dependence on the ^{3}He/^{4}He ratio.

Subject headings: Sun: flares — Sun: particle emission

On-line material: machine-readable tables

1. INTRODUCTION AND MOTIVATION

Measurements of the elemental and isotopic composition of energetic nuclei from solar energetic particle (SEP) events can provide information about the sources of the ions and their acceleration. SEP events have been classified into two main types: impulsive and gradual (Reames 1995a). In gradual events, which have a duration on the order of days, the abundances of heavy SEPs vary from event to event, exhibiting fractionation patterns ordered by their charge-to-mass ratios Q/M (e.g., Breneman & Stone 1985). The acceleration of the nuclei during these events is understood to occur at shock waves that are driven by coronal mass ejections (CMEs; Gosling 1993; Kahler 1992, 1994; Reames 1999). On average, the heavy-element composition of SEP material from gradual events reflects that of the corona (see, e.g., Cook, Stone, & Vogt 1984).

The abundances of heavy SEP elements from gradual events with first ionization potential (FIP) less than 10 eV are characterized by average enhancements, when normalized to photospheric values, over elements with FIP greater than 10 eV by a factor of ~4 (Cook et al. 1984). These enhancements are called the "FIP effect" or "FIP step" and are present in the corona (e.g., Meyer 1985), as well as in the slow solar wind (Geiss et al. 1995).

Unlike gradual events, impulsive SEP events commonly contain enhancements in Fe (~10 times) and in Ne, Mg, and Si (~3 times) relative to coronal abundances (Mason et al. 1986; Reames, Meyer, & von Rosenvinge 1994). In addition, impulsive events frequently have ^{3}He/^{4}He ratios that can be up to 3–4 orders of magnitude (e.g., Reames et al. 1994) larger than the solar wind value of 4×10^{-4} (Gloeckler & Geiss 1998). They are observed to be associated with ~keV electron emission from the Sun (Reames et al. 1985) and with impulsive X-ray flares (e.g., Reames et al. 1988). While the acceleration mechanism in impulsive events may occur after preheating by ion cyclotron wave resonances (Fisk 1978; Temerin & Roth 1992) or could be entirely due to cascading Alfvén waves (Miller 1998), the exact physical processes involved are not presently well understood. However, it is widely accepted that SEPs from impulsive events originate from localized active regions on the Sun, rather than from a more diffuse region in the corona or interplanetary space as in the shock-accelerated gradual events.

Since SEPs from impulsive events have been shown to originate from source ions with coronal and not photospheric composition (Reames et al. 1994), it follows directly that just as in gradual events, the FIP effect should be present in SEP abundances from impulsive events. Previously, the magnitude of this FIP effect in impulsive SEP events has not been closely examined. The topic is of interest for several reasons. First, the FIP step in large gradual SEP events has been shown to vary in magnitude from event to event (Garrard & Stone 1994; Mewaldt et al. 2000, 2002). This variation has not been investigated in small or impulsive SEP events. Second, it has been shown with spectroscopic measurements that the magnitude of the FIP step in selected active regions increases steadily with the age of the region (Widing & Feldman 2001). Since impulsive SEPs are thought to originate from active regions, it is important to measure the magnitude of the FIP effect in SEPs associated with events from these regions. Finally, the FIP step in active regions on the Sun has been measured spectroscopically to be as high as ~15 (Widing & Feldman 1992), which is much higher than the typical size of the FIP step measured in the corona, solar wind, and gradual SEP events.

[1] Jet Propulsion Laboratory, 4800 Oak Grove Avenue, Pasadena, CA 91109.
[2] The Aerospace Corporation, M2/260, P.O. Box 92957, Los Angeles, CA 90009-2957.
[3] California Institute of Technology, MC 220-47, 1200 East California Boulevard, Pasadena, CA 91125.
[4] NASA Goddard Space Flight Center, 8800 Greenbelt Road, Greenbelt, MD 20771.
[5] University of Maryland Department of Physics, College Park, MD 20742.
[6] Florida Institute of Technology, Department of Physics and Space Sciences, 150 West University Boulevard, Melbourne, FL 32901.

In this paper we have examined the heavy-element and He isotope content of 39 small SEP events, using data from the Solar Isotope Spectrometer (SIS; Stone et al. 1998) and the Ultra–Low-Energy Isotope Spectrometer (ULEIS; Mason et al. 1998) on the *Advanced Composition Explorer* (*ACE*). SIS is composed of two silicon solid-state detector telescopes that are sensitive to the nuclear charge and mass of ~10–100 MeV nucleon^{-1} ions with $2 < Z \lesssim 30$. The ULEIS instrument is a high-resolution time-of-flight mass spectrometer that measures the mass of ions with $2 < Z \lesssim 28$, at energies from ~45 keV nucleon^{-1} to a few MeV nucleon^{-1}. With data from these instruments, we have categorized the events according to their ^{3}He/^{4}He ratios and measured the average heavy-element content in each group. In addition, we have determined the Q/M- and FIP-dependent fractionation in each event using a model of a power law in Q/M, times a step function in FIP (Garrard & Stone 1994; Mewaldt et al. 2000, 2002). We have also examined the effect of replacing Q/M with Z in the model, as Z is expected to have a monotonic relationship with Q/M.

2. EVENT CHARACTERISTICS

2.1. *Event Selection Criteria*

The 39 SEP events selected for this study were chosen according to several criteria. First, a set of 171 days between 1998 April 3 and 2002 February 26 was identified using SIS data by requiring that the daily averaged 11.0–26.5 MeV nucleon^{-1} Fe and/or 8.6–19.3 MeV nucleon^{-1} Mg intensities be greater than a threshold of 5.0×10^{-7} particles (cm^2 sr s MeV nucleon^{-1})$^{-1}$, and that they not overlap with any large SEP events. For the purposes of this study, "large" SEP events, many of which have been previously reported (see, e.g., Leske et al. 2001), typically have daily averaged 8.6–19.3 MeV nucleon^{-1} Mg intensities that exceed $\sim 5 \times 10^{-6}$ particles (cm^2 sr s MeV nucleon^{-1})$^{-1}$ at the peak of the event. The lower threshold of 5.0×10^{-7} particles (cm^2 sr s MeV nucleon^{-1})$^{-1}$ was chosen simply to avoid including small SEP events that were difficult to distinguish statistically from background intensities at these energies. Figure 1 shows an example of a small event from this study, compared to a representative large SEP event.

With the set of 171 days selected according to Fe and Mg content as described above, the hourly averaged ~3–5 MeV nucleon^{-1} He intensities from SIS were examined on and around these days. Time periods were identified subjectively that appeared to define complete small SEP events, from onset to termination in the ~3–5 MeV nucleon^{-1} He intensity. One or two events whose intensity versus time profiles suggested that the ^{4}He and ^{3}He intensities originated from different SEP events were avoided, thereby excluding time periods with misleading values of ^{3}He/^{4}He. However, because of the frequent occurrence of these small SEP events, it is likely that up to one-third of the selected events contain multiple injections, probably from the same region on the Sun. This is not expected to alter the conclusions of the study.

The final set of 39 small SEP events, with the times of their occurrences and 0.5–2.0 ^{3}He/^{4}He ratios from ULEIS, are shown in Table 1. The ^{3}He/^{4}He ratios are derived from ULEIS instead of SIS because the ULEIS instrument operates in a lower energy range and thus is exposed to higher particle intensities. Also noted in Table 1 are the events that show velocity dispersion or have interplanetary shocks, both of which will be discussed below. The average heavy-element intensities for each of the 39 events in the study have been tabulated in the Appendix.

The sizes of the 39 small SEP events are depicted in the histograms of Figure 2. Shown in the figure are the average intensities of C, Mg, and ^{4}He, as well as the distribution of the average ^{3}He/^{4}He ratios in the fourth panel. The histogram of ^{4}He indicates that most of the SEP events had an average 4.5–5.5 MeV nucleon^{-1} ^{4}He intensity that was between 0.001 and 0.1 particles (cm^2 sr s MeV nucleon^{-1})$^{-1}$. For comparison, the past study of 228 ^{3}He-rich SEP events by Reames et al. (1994) included events with average 1.3–1.6 MeV nucleon^{-1} ^{3}He intensities between ~0.001 and ~0.1 particles (cm^2 sr s MeV nucleon^{-1})$^{-1}$. Using the distribution of ^{3}He/^{4}He ratios (~0.1–10) reported for the 228 events in the study, and assuming a power-law index in the energy spectrum of ~ -4, one finds that the ^{4}He intensities in the 228 events from Reames et al. (1994) are generally smaller than those from this study (shown in Fig. 2). All of the 39 events in this study are larger than approximately 90% (or 80%, if one assumes a power-law index of -3) of the 228 events discussed in the work by Reames et al. (1994).

Because of the simplicity of our selection criteria (essentially a threshold on the heavy ion intensities), there are at least two types of energetic particle events included in our data set. Although we have made preliminary observations concerning the origin and classification of the events, an extensive treatment of each small SEP event is beyond the scope of this work. However, three characteristics of the

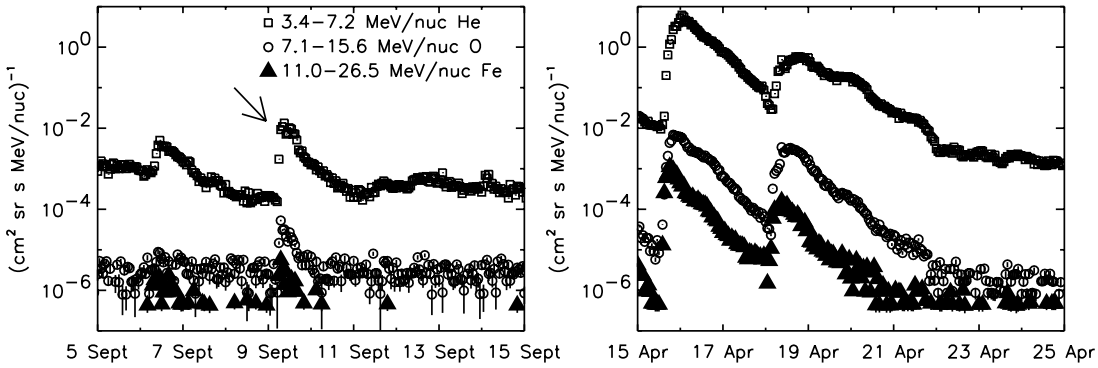

FIG. 1.—Two plots showing hourly averaged particle intensities from a typical small SEP event in this study (*left panel*), and from the large gradual SEP events of 2001 April (*right panel*). The arrow in the top panel indicates the onset of the small SEP event (1998 September 9).

TABLE 1
CHARACTERISTICS OF THE 39 SMALL SEP EVENTS INCLUDED IN THIS STUDY

Event Number	Date	Days	0.5–2.0 MeV nucleon^{-1} ^{3}He/^{4}He	V-disp.	Shock
1	1998 Apr 3	93.1–104.8	$8.15 \pm 0.42 \times 10^{-3}$	...	...
2	1998 Apr 29	119.7–121.3	$2.62 \pm 1.45 \times 10^{-3}$	...	F
3	1998 May 1	121.3–122.2	$7.01 \pm 2.70 \times 10^{-3}$	...	F
4	1998 May 27	147.4–148.6	$4.00 \pm 0.23 \times 10^{-2}$	Yes	...
5	1998 Jun 16	167.7–170.6	$1.60 \pm 0.34 \times 10^{-3}$	Yes	F
6	1998 Sep 8	251.6–254.2	$2.10 \pm 0.06 \times 10^{-1}$	Yes	...
7	1998 Sep 27	270.2–272.1	$1.16 \pm 0.02 \times 10^{-1}$	...	...
8	1998 Oct 21	294.1–297.0	$3.03 \pm 0.87 \times 10^{-3}$	...	F
9	1998 Nov 5	309.7–311.7	$<1.1 \times 10^{-3}$	Yes	...
10	1998 Nov 7	311.7–316.4	$2.16 \pm 0.10 \times 10^{-2}$	...	F
11	1998 Nov 23	327.5–334.9	$3.22 \pm 0.38 \times 10^{-3}$	...	...
12	1999 May 27	147.3–148.4	$1.30 \pm 0.12 \times 10^{-1}$	...	...
13	1999 Jun 21	172.7–176.0	$3.50 \pm 0.17 \times 10^{-2}$	...	...
14	1999 Nov 17	321.8–327.3	$5.62 \pm 0.48 \times 10^{-3}$	...	...
15	1999 Dec 28	362.0–364.2	$1.58 \pm 0.07 \times 10^{-1}$	...	...
16	2000 Jan 9	9.2–13.5	$1.21 \pm 0.10 \times 10^{-2}$	...	F
17	2000 Mar 7	67.2–68.8	$3.24 \pm 0.21 \times 10^{-1}$	Yes	...
18	2000 Mar 22	82.4–87.2	$1.48 \pm 0.29 \times 10^{-3}$	...	R
19	2000 May 1	122.3–123.0	$6.62 \pm 0.43 \times 10^{-2}$	Yes	...
20	2000 May 4	125.3–126.7	$6.38 \pm 1.11 \times 10^{-2}$	...	...
21	2000 May 15	136.7–138.8	$1.57 \pm 0.46 \times 10^{-3}$	...	...
22	2000 May 17	138.8–140.7	$2.08 \pm 0.46 \times 10^{-3}$	...	F
23	2000 May 23	144.7–147.9	$2.06 \pm 0.05 \times 10^{-1}$	...	...
24	2000 Jun 15	167.8–169.1	$2.46 \pm 0.17 \times 10^{-2}$	Yes	...
25	2000 Jun 17	169.2–172.9	$9.84 \pm 0.71 \times 10^{-3}$	Yes	...
26	2000 Jun 23	175.3–177.2	$1.97 \pm 0.16 \times 10^{-2}$	...	F
27	2000 Jun 25	177.2–180.6	$2.80 \pm 0.38 \times 10^{-3}$	...	...
28	2000 Aug 11	224.0–225.4	$6.29 \pm 1.54 \times 10^{-3}$	...	F
29	2000 Aug 12	225.4–226.6	$8.70 \pm 0.72 \times 10^{-3}$	...	...
30	2000 Aug 13	226.6–228.6	$1.43 \pm 0.38 \times 10^{-3}$	...	F
31	2001 Mar 10	69.2–73.9	$4.47 \pm 0.26 \times 10^{-1}$	...	...
32	2001 Mar 25	84.5–87.4	$5.31 \pm 0.75 \times 10^{-3}$	...	F
33	2001 Apr 26	116.4–119.6	$3.16 \pm 0.53 \times 10^{-3}$	...	F
34	2001 May 20	140.3–143.3	$1.52 \pm 0.42 \times 10^{-2}$	...	...
35	2001 Jun 15	166.6–167.3	$3.54 \pm 1.20 \times 10^{-3}$	...	...
36	2001 Jun 16	167.3–169.4	$3.02 \pm 0.71 \times 10^{-3}$	...	...
37	2001 Jul 19	200.6–203.4	$2.80 \pm 1.68 \times 10^{-3}$	...	...
38	2001 Sep 10	253.4–255.7	$1.38 \pm 0.07 \times 10^{-1}$	...	...
39	2002 Feb 20	51.0–57.0	$3.00 \pm 0.30 \times 10^{-2}$	...	...

NOTES.— Shown in the table from left to right are the event numbers, the event times, the 0.5–2.0 MeV nucleon^{-1} ^{3}He/^{4}He ratios from ULEIS, one column noting velocity dispersion in the ~0.1–10 MeV nucleon^{-1} ion data from ULEIS, and one column indicating interplanetary shocks detected using the MAG and SWEPAM instruments (see text). Forward shocks are denoted by "F" and reverse by "R." Ellipses indicate an event without clear velocity dispersion (fifth column) or an event in which there was no shock detected at *ACE* (sixth column). The event times used to calculate the ^{3}He/^{4}He ratios from ULEIS are displaced by 2.7 hr from the times shown in the table to account for the difference in energy ranges between the SIS and ULEIS instruments. Table 2 is also available in machine-readable form in the electronic edition of the *Astrophysical Journal*.

events that have been investigated are the velocity dispersion of the ~0.1–1 MeV nucleon^{-1} incident particles, the coincident 50–100 keV electron activity, and the passing of interplanetary shocks during the events.

These three features have been examined using data from additional instruments on board *ACE*. We have checked for velocity dispersion in each event using data from the ULEIS instrument.[7] We find that eight of the events show clear velocity dispersion. These events are noted in Table 1. Second, we have examined the coincident 50–100 keV electron activity measured using the Electron, Proton, and Alpha Monitor (EPAM) on *ACE* (Gold et al. 1998).[8] We find that there are increases in the 50–100 keV electron intensity during all of the small SEP events. Finally, in Table 1 we have noted the instances in which interplanetary shocks passed *ACE* during the 39 small SEP events, using data from the Magnetic Field Experiment (MAG) and Solar Wind Electron Proton Alpha Monitor (SWEPAM) instruments. These observations of the shocks and their characteristics were taken from the summary by C. W. Smith, H. Qiang, & R. M. Skoug.[9]

[7] See http://www.srl.caltech.edu/ACE/ASC/DATA/ftp/pub/ace/level3/uleis/swoosh.html.

[8] See http://www.srl.caltech.edu/ACE/ASC/level2/lvl2DATA_EPAM.html.

[9] See http://www.bartol.udel.edu/~chuck/ace/ACElists/obs_list.html.

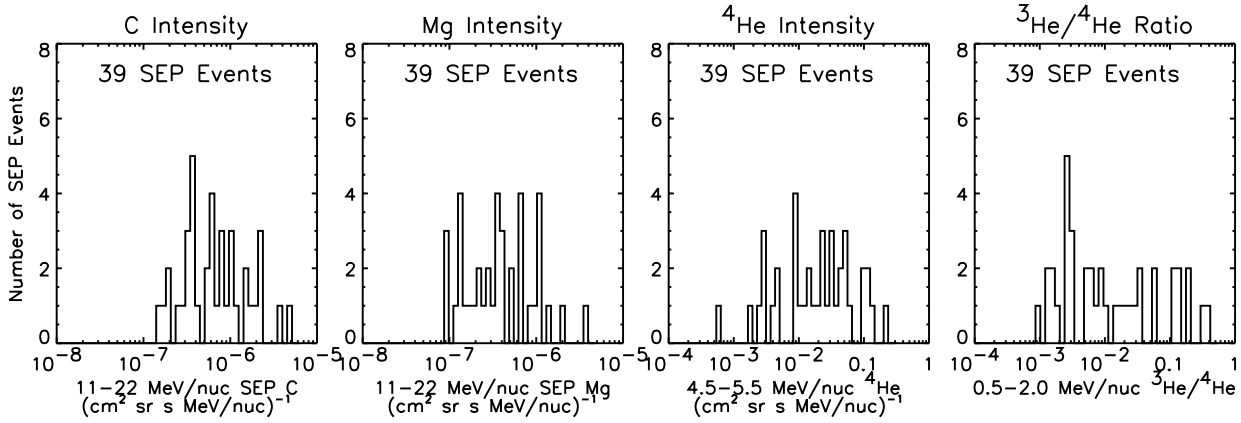

FIG. 2.—Histograms of average intensities of the ~11–22 MeV nucleon^{-1} SEP C (*first panel*) and Mg (*second panel*), and 4.5–5.5 MeV nucleon^{-1} ^{4}He (*third panel*), measured using SIS, for the 39 SEP events in this study. The fourth panel shows a histogram of the 0.5–2.0 MeV nucleon^{-1} ^{3}He/^{4}He ratios, also for the 39 events in the study.

For several reasons, we have attributed event 18 to a corotating interaction region (CIR; see, e.g., Fisk & Lee 1980). This event was observed by Smith et al.[10] to have a reverse shock. In addition, it shows no evidence of velocity dispersion in the ~0.1–1 MeV nucleon^{-1} ULEIS data. It occurs in coincidence with an increase in the solar wind speed from the SWEPAM data, and, as shown in the Appendix, has an enhanced 11–22 MeV nucleon^{-1} C/O ratio ($1.6 \pm 0.2 \times$ coronal). There are also increased ~MeV He fluxes at *ACE* approximately 27 days before and 27 days after the event. Since each of these features are thought to be characteristic of CIRs (see, e.g., Mason et al. 1999b), we believe it is likely that the event is associated with a CIR.

The set of 39 small events was subdivided into three categories according to the ~0.5–2.0 MeV nucleon^{-1} ^{3}He/^{4}He ratios. As shown in the fourth panel of Figure 2, 24 of the 39 events had ^{3}He/^{4}He ratios less than 0.02 ("^{3}He-poor" events), while seven had ^{3}He/^{4}He ratios that were between 0.02 and 0.1 ("moderately ^{3}He-rich"). Finally, eight of the events had ^{3}He/^{4}He ratios greater than 0.1, and were designated "^{3}He-rich". In general, the ^{3}He-poor events had ^{3}He/^{4}He ratios that averaged, without weighting, to about 0.5%. While the nomenclature "^{3}He-poor" may appear misleading for these events, given that their ^{3}He/^{4}He ratios are up to ~50 times that of the solar wind, we have chosen to use it as a convenient label for the purposes of this study.

Although the unweighted average 0.5–2.0 MeV nucleon^{-1} ^{3}He/^{4}He ratio in the ^{3}He-rich, moderately ^{3}He-rich, and ^{3}He-poor groups is ~21%, ~4%, and ~0.5%, respectively, and impulsive SEP events are expected to have higher ^{3}He/^{4}He ratios than gradual events, one cannot assume that the ^{3}He-rich events are impulsive and the ^{3}He-poor events are gradual. More specifically, it is possible that while the ^{3}He-rich events contain a relatively large fraction of material that was originally accelerated in impulsive SEP events, they may also have been influenced by other physical processes in interplanetary space. For example, Mason, Mazur, & Dwyer (1999a) suggested that residual material from past impulsive SEP events may provide a source population for further acceleration by CME-driven shocks associated with gradual events. Observations of SEP composition during large gradual events (Cohen et al. 1999, 2000; Mason et al. 1999a; Wiedenbeck et al. 2000; Tylka et al. 2001) and during times of lower solar activity (Richardson et al. 1990; Desai et al. 2001; Slocum et al. 2002) appear to be consistent with this idea.

[10] See footnote 9.

2.2. *Heavy-Element Composition*

Average energy spectra were measured for C, N, O, Ne, Na, Mg, Al, Si, S, Ar, Ca, and Fe for each of the three SEP event subsets. These spectra were calculated by summing the total number of particles in all events for each subset, dividing by the total amount of instrument livetime, and finally dividing by the geometry factor (in units of cm^2 sr) and the appropriate energy interval. Next, each average spectrum was corrected for contributions from Galactic cosmic rays (GCRs) and anomalous cosmic rays (ACRs; e.g., Fisk et al. 1998) as described in § 3. Figure 3 and Table 2 show the resulting ~11–22 MeV nucleon^{-1} relative abundances of 11 heavy elements with respect to C, normalized to coronal abundances (Reames 1998), for the ^{3}He-rich, moderately ^{3}He-rich, and ^{3}He-poor SEP event subsets.

From Figure 3, it is apparent that while the heavy-element composition of the ^{3}He-poor data set generally reflects coronal composition as derived from gradual SEP

TABLE 2

NUMERICAL VALUES OF THE 11.0–21.8 MeV nucleon^{-1} HEAVY-ELEMENT ABUNDANCES FROM SIS, PLOTTED IN FIG. 3

Element/C	^{3}He/^{4}He < 0.02	$0.02 < ^3$He/^{4}He < 0.10	^{3}He/^{4}He > 0.10
N	0.95 ± 0.14	1.42 ± 0.20	0.94 ± 0.23
O	0.88 ± 0.07	0.91 ± 0.08	0.98 ± 0.13
Ne	0.79 ± 0.10	1.38 ± 0.18	2.03 ± 0.33
Na	1.15 ± 0.43	1.40 ± 0.57	2.30 ± 1.04
Mg	1.11 ± 0.10	1.40 ± 0.16	1.65 ± 0.24
Al	1.02 ± 0.31	1.76 ± 0.56	2.42 ± 0.89
Si	1.04 ± 0.11	1.65 ± 0.20	2.21 ± 0.34
S	1.02 ± 0.18	1.46 ± 0.30	3.35 ± 0.71
Ar	1.26 ± 0.72	4.00 ± 1.58	7.56 ± 3.13
Ca	1.25 ± 0.37	2.13 ± 0.66	4.79 ± 1.49
Fe	1.07 ± 0.13	3.30 ± 0.39	5.86 ± 0.83

NOTE.—The data are shown as dimensionless ratios with the form $(X/C)/(X/C)_{Coronal}$.

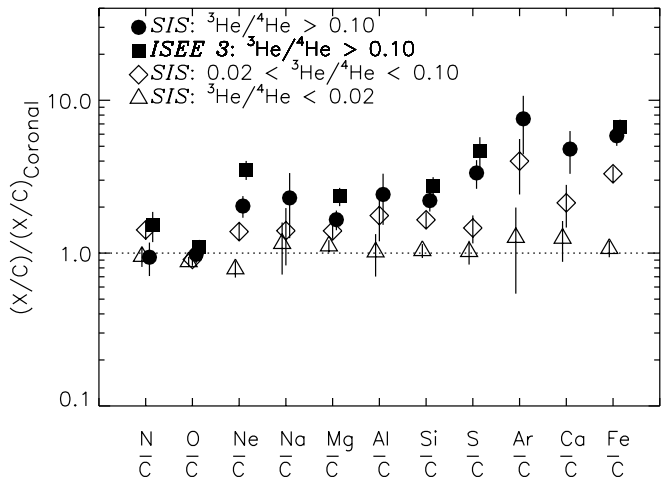

FIG. 3.—Average 11.0–21.8 MeV nucleon^{-1} abundances of 11 heavy elements with respect to C, normalized to coronal abundances (Reames 1998), for the ^{3}He-rich (*filled circles*), moderately ^{3}He-rich (*open diamonds*), and ^{3}He-poor (*open triangles*) data sets. Uncertainties shown on the data points from SIS include 2 standard deviations of statistical error. Also shown are the 1.9–2.8 MeV nucleon^{-1} abundances (*filled squares*) for seven heavy elements reported for 228 impulsive SEP events measured using ISEE-3 for which the 1.3–1.6 MeV nucleon^{-1} ^{3}He/^{4}He ratio was greater than 0.1 (Reames et al. 1994). Uncertainties on the ISEE-3 points include 2 standard deviations of combined statistical error and population spread.

event observations (Reames 1998), the moderately ^{3}He-rich and ^{3}He-rich data sets from SIS contain enhancements relative to C in most of the measured elements heavier than O. Also shown in the figure are the 1.9–2.8 MeV nucleon^{-1} abundances measured for the sample of 228 ^{3}He-rich (1.3–1.6 MeV nucleon^{-1} ^{3}He/^{4}He > 0.1) events from ISEE-3 (Reames et al. 1994). The ^{3}He-rich abundances from SIS are in reasonably good agreement with the ISEE-3 data, especially considering that the energy intervals and the sizes of the two data sets are different (228 ISEE-3 events compared to eight SIS events). There is, however, a significant difference in the Ne/C ratio in ^{3}He-rich events observed using ISEE-3 (3.51 ± 0.50) and SIS (2.03 ± 0.33).

In comparing the above Ne/C ratio from SIS (2.03 ± 0.33) to other past studies of ^{3}He-rich events, one finds better agreement than with the value from Reames et al. (1994). In a study of 139 impulsive SEP events by Reames (1993, 1995b), the average enhancement of Ne/C over the SEP-derived coronal value was found to be 2.61 ± 0.41, reported with 2 standard deviations of uncertainty. Mason et al. (2002b) studied 14 ^{3}He-rich events and found the Ne/C enhancement to be 2.96 ± 0.82, with 1 standard deviation of uncertainty. Each of these other measurements are in better agreement with the Ne/C ratio found in this study. Finally, it has been shown recently that there can be great variability in the enhancement patterns of heavy elements in ^{3}He-rich events (Mason et al. 2002a). Thus, it is probably not surprising that the Ne/C ratio from SIS in Figure 3 differs from that of ISEE-3.

3. SOLAR QUIET-TIME SPECTRA

An important step in deriving the SEP intensities in each small event is the subtraction of GCRs and ACRs from the total particle spectra. Such a correction is necessary because in this study the normalization for the heavy-element abundances in each event is based on the C intensity, and the intensity of C between the small SEP events is nonnegligible at energies of ~11–22 MeV nucleon^{-1}. The magnitude of this adjustment to the C intensity can be as high as ~30% in some events. Likewise, the abundances of other heavy elements require a similar correction. Figure 4 shows an example of the total C, N, O, and Ne spectra from event 5, along with the estimated ACR+GCR spectra for comparison. Event 5 is typical of approximately one-third of the data set; the remaining events are large enough not to be affected significantly by the correction for ACRs and GCRs.

The combined GCR and ACR spectra, such as those shown in Figure 4, have been estimated in each event using SIS measurements from 299 days of low solar activity between 1998 April 9 and 2002 February 14. The 299 days were identified by examining the proton intensities from the EPAM instrument[11] on board *ACE* and requiring that the daily averaged 1.06–4.75 MeV proton intensity be less than 0.16 (cm^2 sr s MeV)$^{-1}$. Most of these quiet days did not overlap with any of the small SEP events, with the exception of the first day of event 17. (Event 17 peaked during the last third of 2000 March 7 and had relatively small proton intensities.) Next, the 299 days were grouped chronologically into four time periods of relatively constant solar modulation, based on inspection of ~60–90 MeV nucleon^{-1} O intensities from SIS. These time periods were 1998 April 9 through 1998 November 24, 1998 November 25 through 2000 January 13, 2000 January 14 through 2001 July 31, and 2001 August 1 through 2002 February 13. For each of the four time periods, the average heavy-element spectra were extracted from the daily measurements.

[11] See footnote 8.

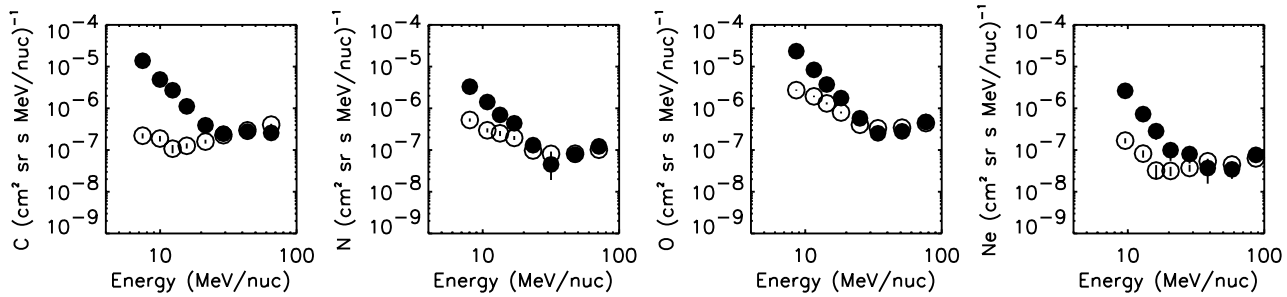

FIG. 4.—Elemental spectra of C, N, O, and Ne for event 5 (1998 June 16). The filled circles represent the average particle intensities measured with the SIS instrument during the event. The open circles show the estimated, combined contribution from ACRs and GCRs to the measured particle intensities (see text). The uncertainties plotted are statistical in nature.

Next, for each small SEP event the heavy-element spectra were corrected by subtracting the low solar activity intensities corresponding to the time period in which the small event occurred. Similarly, when the spectra from the small SEP events were summed, the average low solar activity intensities were weighted with the temporal fraction of the small SEP events that occurred during each of the three time periods and were then summed for subtraction from the total spectra.

4. FRACTIONATION

It has been known for years that the elemental fractionation of ions observed in large gradual SEP events is governed by physical processes that depend on the charge to mass ratio Q/M of the particles (e.g., Breneman & Stone 1985). Furthermore, as mentioned previously, it is well established that in gradual events the abundances of elements with FIP less than 10 eV are enhanced (when normalized to oxygen) relative to photospheric values (Cook et al. 1984; Breneman & Stone 1985; Meyer 1985) by a factor that varies from event to event (Garrard & Stone 1994; Mewaldt et al. 2000, 2002).

In order to study the effects of elemental fractionation in Q/M, Z, and FIP in the 39 small SEP events of this study, it is necessary to examine the data one event at a time rather than in groups, as in the previous sections. By doing so, the type and degree of fractionation in each event can be measured independently of the rest of the data set. This is important because the degree of each type of fractionation present may vary considerably from event to event.

Several challenges arise when examining the fractionation in the small events. Because there are at least two types of events in the data set, it is difficult to invoke one mathematical model that completely describes all of the SEP abundances. Also, since there are no charge state measurements for the small SEP events in this energy range (11–22 MeV nucleon^{-1}), any model based on Q/M will have an obvious uncertainty in the assumed charge states Q. Additional uncertainties come from the suggestion that the apparent FIP fractionation observed in coronal material is actually "FIT" (first ionization time) fractionation (e.g., Geiss 1998). However, since FIP and FIT are related, and FIT is strongly model-dependent, we have used FIP in this paper. Finally, the event intensities in this data set are necessarily small and thus have sizeable statistical uncertainties.

Although we find that a model consisting of a power law in Q/M, or Z, times a step function in FIP does not incorporate all of the variability observed in many events, it is adequate for the purposes of this study. This technique is identical to that used in several past studies of large gradual SEP events (Garrard & Stone 1994; Mewaldt et al. 2000, 2002). Previously, the technique has not been applied to SEP abundances in impulsive events. This is partly because statistics are generally low in impulsive SEP events and because the heavy isotope enhancements found in impulsive events are not always consistent with a power-law dependence on Q/M (Dwyer et al. 2001). However, it is appropriate to investigate the range of applicability of a power-law dependence in Q/M or Z to the heavy-element abundances in impulsive events. Note that Q/M and Z are closely related because Q increases monotonically with increasing Z.

In the absence of charge state measurements for 11–22 MeV nucleon^{-1} ions from small SEP events, the mean charge states Q in each event have been estimated from the Fe/C ratio. Specifically, Moebius et al. (2000) showed that at ~MeV nucleon^{-1} energies $Q_{\rm Fe}$ increased approximately linearly with the log of the Fe/O ratio in a survey of gradual and impulsive events. The results of the study indicated that the highest values of $Q_{\rm Fe}$ occurred in SEP events with very large Fe/O ratios ($\geq 10 \times$ coronal) and were consistent with temperatures in a thermal equilibrium model of ~10 MK. The lowest values of $Q_{\rm Fe}$ came from events with composition similar to that of the corona and were consistent with source temperatures of 1–3 MK. We have applied these results to our study by assuming that $Q_{\rm Fe}$ in each event varies linearly with the log of the Fe/C ratio:

$$Q_{\rm Fe} = \ln\left[\frac{\rm Fe/C}{(\rm Fe/C)_{COR}}\right]\frac{Q_2(T_2) - Q_1(T_1)}{\ln(10)} + Q_1(T_1)\ . \quad (1)$$

In the equation above Q_1 is defined as the mean charge state of Fe in a thermal equilibrium model (Mazzotta et al. 1998) at temperature $T_1 = 2$ MK and is applied to events with $(\rm Fe/C)/(Fe/C)_{COR} = 1$. Similarly, Q_2 is the mean charge state of Fe at T_2 and is applied to events with $(\rm Fe/C)/(Fe/C)_{COR} = 10$. The values of T_2 were chosen separately to be 4, 6, 8, and 10 MK in order to evaluate the effects of four temperature spreads (T_1 through T_2) on the analysis. Once $Q_{\rm Fe}$ in each event was estimated from equation (1), the corresponding temperature and mean charge states of the other heavy elements were determined from the thermal equilibrium model.

With the above points in mind, we have calculated the ~11–22 MeV nucleon^{-1} heavy-element abundances with respect to C, normalized to photospheric abundances (Grevesse & Sauval 1998), for each of the 39 SEP events in the data set. We have investigated the dependence of the abundance ratios on Q/M or Z, fitting the abundances of each event with the functional form of a power law times a step function in FIP:

$$f(Q/M \text{ or } Z) = \begin{cases} A_1 A_2 (Q/M \text{ or} Z)^{\gamma} & \text{if FIP} < 10 \text{ eV}, \\ A_2 (Q/M \text{ or } Z)^{\gamma} & \text{if FIP} > 10 \text{ eV}, \end{cases} \quad (2)$$

where the FIP factor is defined as A_1. Sulfur is not included in any of the fits because its FIP value is approximately 10 eV, in the transition between the high FIP and low FIP elements. The fit values for γ and A_1 for each event, using either Q/M at four temperature ranges or Z, appear in Table 3.

Figure 5 shows examples of fits with power laws in Q/M and in Z for four small SEP events, assuming a temperature spread (T_1 to T_2) of 2–4 MK over the whole data set. The four events shown in the figure have been chosen to display a variety of values, both positive and negative, of the power-law indices from the fits. The uncertainties shown in the plots of Figure 5 include the statistical uncertainty in the abundances of element "X" in the SEP event and the uncertainty in X in the photosphere. The uncertainty in C is not included because it is a factor common to each data point in the plots and therefore does not affect the calculation of the FIP step magnitudes or power-law slopes.

Figure 6 summarizes the results for similar fits to each of the small events, as well as for 13 "typical" large SEP

TABLE 3
CHARACTERISTICS OF THE 39 SMALL SEP EVENTS INCLUDED IN THIS STUDY

Event Number	$FIP_{Q/M}$ (2–4 MK)	$\gamma_{Q/M}$ (2–4 MK)	$FIP_{Q/M}$ (2–6 MK)	$\gamma_{Q/M}$ (2–6 MK)	$FIP_{Q/M}$ (2–8 MK)	$\gamma_{Q/M}$ (2–8 MK)	$FIP_{Q/M}$ (2–10 MK)	$\gamma_{Q/M}$ (2–10 MK)	FIP_Z	γ_Z
1.....	2.1 ± 0.3	0.6 ± 0.5	2.1 ± 0.3	0.6 ± 0.5	2.1 ± 0.3	0.6 ± 0.5	2.1 ± 0.3	0.6 ± 0.5	2.5 ± 0.5	-0.4 ± 0.3
2.....	3.2 ± 0.9	-1.2 ± 0.6	3.2 ± 1.0	-1.3 ± 0.7	3.2 ± 0.9	-1.4 ± 0.7	2.9 ± 0.9	-1.6 ± 0.7	2.9 ± 1.2	0.6 ± 0.4
3.....	3.5 ± 1.1	-0.8 ± 0.7	3.5 ± 1.0	-0.9 ± 0.7	3.5 ± 1.0	-0.9 ± 0.7	3.4 ± 1.0	-1.0 ± 0.7	3.3 ± 1.4	0.4 ± 0.4
4.....	5.5 ± 1.0	-0.8 ± 0.5	5.4 ± 1.0	-0.8 ± 0.5	5.4 ± 1.1	-0.8 ± 0.5	5.5 ± 1.1	-0.7 ± 0.6	4.5 ± 1.1	0.5 ± 0.3
5.....	5.1 ± 0.6	0.8 ± 0.4	5.1 ± 0.6	0.8 ± 0.4	5.1 ± 0.6	0.8 ± 0.4	5.1 ± 0.6	0.8 ± 0.4	6.4 ± 1.2	-0.5 ± 0.2
6.....	5.5 ± 1.0	-2.2 ± 0.5	5.7 ± 1.1	-2.1 ± 0.5	5.9 ± 1.1	-2.2 ± 0.5	6.1 ± 1.1	-2.7 ± 0.6	4.2 ± 0.9	1.2 ± 0.2
7.....	4.1 ± 0.5	-3.2 ± 0.3	3.8 ± 0.5	-3.4 ± 0.3	3.9 ± 0.5	-3.6 ± 0.3	4.1 ± 0.5	-4.2 ± 0.4	2.6 ± 0.4	1.7 ± 0.2
8.....	6.2 ± 2.5	1.6 ± 2.3	6.2 ± 2.5	1.6 ± 2.3	6.2 ± 2.5	1.6 ± 2.3	6.2 ± 2.5	1.6 ± 2.3	9.5 ± 6.9	-1.0 ± 1.1
9.....	4.3 ± 0.5	-0.2 ± 0.3	4.3 ± 0.5	-0.2 ± 0.3	4.2 ± 0.5	-0.2 ± 0.3	4.2 ± 0.5	-0.2 ± 0.3	4.3 ± 0.7	0.0 ± 0.2
10.....	4.7 ± 0.4	0.5 ± 0.2	4.7 ± 0.4	0.5 ± 0.2	4.7 ± 0.4	0.5 ± 0.2	4.7 ± 0.4	0.6 ± 0.2	5.1 ± 0.6	-0.3 ± 0.1
11.....	3.7 ± 0.5	0.8 ± 0.4	3.7 ± 0.5	0.8 ± 0.4	3.7 ± 0.5	0.8 ± 0.4	3.7 ± 0.5	0.8 ± 0.4	4.6 ± 0.9	-0.5 ± 0.2
12.....	4.0 ± 0.8	-1.0 ± 0.5	4.0 ± 0.8	-1.0 ± 0.5	3.9 ± 0.8	-1.0 ± 0.5	3.8 ± 0.8	-1.1 ± 0.6	3.0 ± 0.8	0.7 ± 0.3
13.....	2.6 ± 0.7	0.5 ± 0.9	2.6 ± 0.7	0.5 ± 0.9	2.6 ± 0.7	0.5 ± 0.9	2.6 ± 0.7	0.5 ± 0.9	3.4 ± 1.4	-0.6 ± 0.6
14.....	7.4 ± 1.0	0.5 ± 0.4	7.4 ± 1.0	0.5 ± 0.4	7.4 ± 1.0	0.5 ± 0.4	7.3 ± 1.1	0.4 ± 0.5	8.1 ± 1.6	-0.3 ± 0.3
15.....	4.2 ± 0.5	-2.3 ± 0.3	3.8 ± 0.5	-2.5 ± 0.3	4.1 ± 0.5	-2.4 ± 0.3	4.3 ± 0.5	-2.7 ± 0.3	3.0 ± 0.4	1.2 ± 0.1
16.....	4.3 ± 0.5	0.1 ± 0.3	4.3 ± 0.5	0.1 ± 0.3	4.3 ± 0.5	0.1 ± 0.4	4.3 ± 0.5	0.1 ± 0.4	4.4 ± 0.8	-0.1 ± 0.2
17.....	3.9 ± 0.8	-3.4 ± 0.5	3.4 ± 0.7	-3.7 ± 0.5	3.7 ± 0.8	-3.8 ± 0.5	4.0 ± 0.8	-4.2 ± 0.6	2.8 ± 0.7	1.6 ± 0.2
18.....	3.3 ± 0.7	3.2 ± 1.0	3.3 ± 0.7	3.2 ± 1.0	3.3 ± 0.7	3.2 ± 1.0	3.3 ± 0.7	3.2 ± 1.0	7.4 ± 2.7	-1.9 ± 0.5
19.....	4.7 ± 0.6	-2.9 ± 0.3	5.2 ± 0.6	-2.7 ± 0.3	5.5 ± 0.7	-2.9 ± 0.4	5.8 ± 0.7	-3.5 ± 0.5	3.6 ± 0.5	1.5 ± 0.2
20.....	5.3 ± 1.1	-3.2 ± 0.5	5.6 ± 1.2	-3.3 ± 0.5	5.9 ± 1.2	-3.7 ± 0.6	6.2 ± 1.2	-4.5 ± 0.7	3.8 ± 1.0	1.6 ± 0.2
21.....	3.6 ± 0.5	1.5 ± 0.6	3.6 ± 0.5	1.5 ± 0.6	3.6 ± 0.5	1.5 ± 0.6	3.6 ± 0.5	1.5 ± 0.6	5.3 ± 1.1	-0.9 ± 0.3
22.....	3.4 ± 1.0	1.0 ± 1.4	3.4 ± 1.0	1.0 ± 1.4	3.4 ± 1.0	1.0 ± 1.4	3.4 ± 1.0	1.0 ± 1.4	4.7 ± 2.2	-0.7 ± 0.7
23.....	1.9 ± 0.4	-4.4 ± 0.5	1.9 ± 0.4	-4.7 ± 0.5	2.0 ± 0.4	-5.3 ± 0.6	2.1 ± 0.4	-6.7 ± 0.7	1.1 ± 0.2	2.5 ± 0.2
24.....	7.0 ± 1.3	-1.0 ± 0.5	6.7 ± 1.3	-1.1 ± 0.5	6.4 ± 1.3	-1.2 ± 0.6	6.6 ± 1.4	-1.2 ± 0.6	6.1 ± 1.6	0.5 ± 0.3
25.....	4.9 ± 0.4	-0.6 ± 0.2	4.9 ± 0.4	-0.6 ± 0.2	4.9 ± 0.4	-0.6 ± 0.2	4.8 ± 0.4	-0.7 ± 0.2	4.7 ± 0.6	0.2 ± 0.1
26.....	3.5 ± 0.6	-2.7 ± 0.4	3.1 ± 0.5	-2.8 ± 0.5	3.3 ± 0.6	-2.6 ± 0.5	3.6 ± 0.6	-2.7 ± 0.6	2.2 ± 0.5	1.5 ± 0.2
27.....	5.6 ± 0.7	1.4 ± 0.5	5.6 ± 0.7	1.4 ± 0.5	5.6 ± 0.7	1.4 ± 0.5	5.6 ± 0.7	1.4 ± 0.5	8.9 ± 1.8	-1.1 ± 0.3
28.....	3.8 ± 0.9	0.5 ± 1.4	3.8 ± 0.9	0.5 ± 1.4	3.8 ± 0.9	0.5 ± 1.4	3.8 ± 0.9	0.5 ± 1.4	5.3 ± 2.4	-0.7 ± 0.7
29.....	3.4 ± 0.7	-2.4 ± 0.6	3.2 ± 0.8	-2.4 ± 0.6	3.5 ± 0.9	-2.1 ± 0.7	4.0 ± 1.0	-1.8 ± 0.7	2.5 ± 0.8	1.2 ± 0.3
30.....	6.7 ± 1.5	1.8 ± 0.9	6.7 ± 1.5	1.8 ± 0.9	6.7 ± 1.5	1.8 ± 0.9	6.7 ± 1.5	1.8 ± 0.9	11.1 ± 4.1	-1.2 ± 0.5
31.....	5.0 ± 0.6	-1.3 ± 0.3	4.9 ± 0.6	-1.3 ± 0.3	4.6 ± 0.6	-1.5 ± 0.3	4.2 ± 0.6	-1.8 ± 0.4	4.1 ± 0.7	0.6 ± 0.2
32.....	4.1 ± 0.5	2.0 ± 0.6	4.1 ± 0.5	2.0 ± 0.6	4.1 ± 0.5	2.0 ± 0.6	4.1 ± 0.5	2.0 ± 0.6	6.8 ± 1.5	-1.3 ± 0.3
33.....	5.9 ± 1.1	1.8 ± 0.8	5.9 ± 1.1	1.8 ± 0.8	5.9 ± 1.1	1.8 ± 0.8	5.9 ± 1.1	1.8 ± 0.8	9.3 ± 2.7	-1.1 ± 0.4
34.....	2.5 ± 0.7	-4.6 ± 0.6	2.8 ± 0.8	-4.8 ± 0.6	3.0 ± 0.8	-5.4 ± 0.7	3.0 ± 0.8	-6.8 ± 0.9	1.4 ± 0.5	2.4 ± 0.3
35.....	4.0 ± 0.5	1.0 ± 0.4	4.0 ± 0.5	1.0 ± 0.4	4.0 ± 0.5	1.0 ± 0.4	4.0 ± 0.5	1.0 ± 0.4	5.5 ± 1.0	-0.7 ± 0.2
36.....	4.0 ± 0.4	3.0 ± 0.4	4.0 ± 0.4	3.0 ± 0.4	4.0 ± 0.4	3.0 ± 0.4	4.0 ± 0.4	3.0 ± 0.4	9.2 ± 1.7	-2.0 ± 0.3
37.....	2.6 ± 0.6	-1.1 ± 0.7	2.6 ± 0.6	-1.1 ± 0.7	2.6 ± 0.6	-1.1 ± 0.7	2.6 ± 0.6	-1.1 ± 0.7	2.2 ± 0.7	0.5 ± 0.4
38.....	2.3 ± 0.5	-4.6 ± 0.5	2.2 ± 0.5	-4.8 ± 0.5	2.4 ± 0.5	-5.2 ± 0.6	2.6 ± 0.5	-6.3 ± 0.7	1.5 ± 0.4	2.3 ± 0.2
39.....	3.2 ± 0.3	-2.1 ± 0.2	3.0 ± 0.2	-2.2 ± 0.2	2.6 ± 0.2	-2.6 ± 0.2	2.6 ± 0.2	-3.0 ± 0.2	2.2 ± 0.2	1.2 ± 0.1

NOTES.—Characteristics of the 39 small SEP events included in this study. Shown in the table from left to right are the event numbers and the FIP factors and power-law indices derived using fits with the functional form described by eq. (2). The assumed charge states for the fits in Q/M are taken from a thermal equilibrium model Mazzotta et al. 1998 using temperatures determined using eq. (1). Table 3 is also available in machine-readable form in the electronic edition of the *Astrophysical Journal*.

events measured for comparison using SIS data for the heavy elements and ULEIS data for the He isotope ratios. The 13 large SEP events occurred between 1997 November 6 and 2001 May 10. They were selected from a larger set of gradual events by requiring that the spectral indices of the SEP energy spectra not vary significantly among the elements. The charge states Q in the large SEP events were taken from the mean charge states reported by Labrador et al. (2001). In this study Labrador et al. measured the mean charge states of six elements from five large SEP events, in the energy range $\sim$15–150 MeV nucleon^{-1}. The five large SEP events in the study were divided into two groups according to the Fe/O ratio, and average charge states were reported for each group.

The top two panels of Figure 6 show the power-law indices taken from the fits in the small SEP events (in Q/M and in Z), plotted as a function of the 0.5–2.0 MeV nucleon^{-1} ^{3}He/^{4}He ratio from ULEIS. One clear feature in these two plots is the tendency for the power-law indices in Q/M (Z) to decrease (increase) continuously with the ^{3}He/^{4}He ratio. This trend in the power-law indices reflects the increasing relative abundance of heavy elements with the ^{3}He content and has been seen in recent studies of small SEP events (Ho et al. 2000; Dwyer et al. 2001). Dwyer et al. (2001) concluded that this observation was best explained by a mixing of gradual and impulsive event material, similar to the suggestion by Mason et al. (1999a). Similarly, we believe that the apparent correlation between the heavy-element enhancements and ^{3}He/^{4}He in this study is probably due to mixing of material from gradual and impulsive events. It is also true that the data set contains more than one type of event, which certainly contributes to the spread in power-law indices shown in the figure.

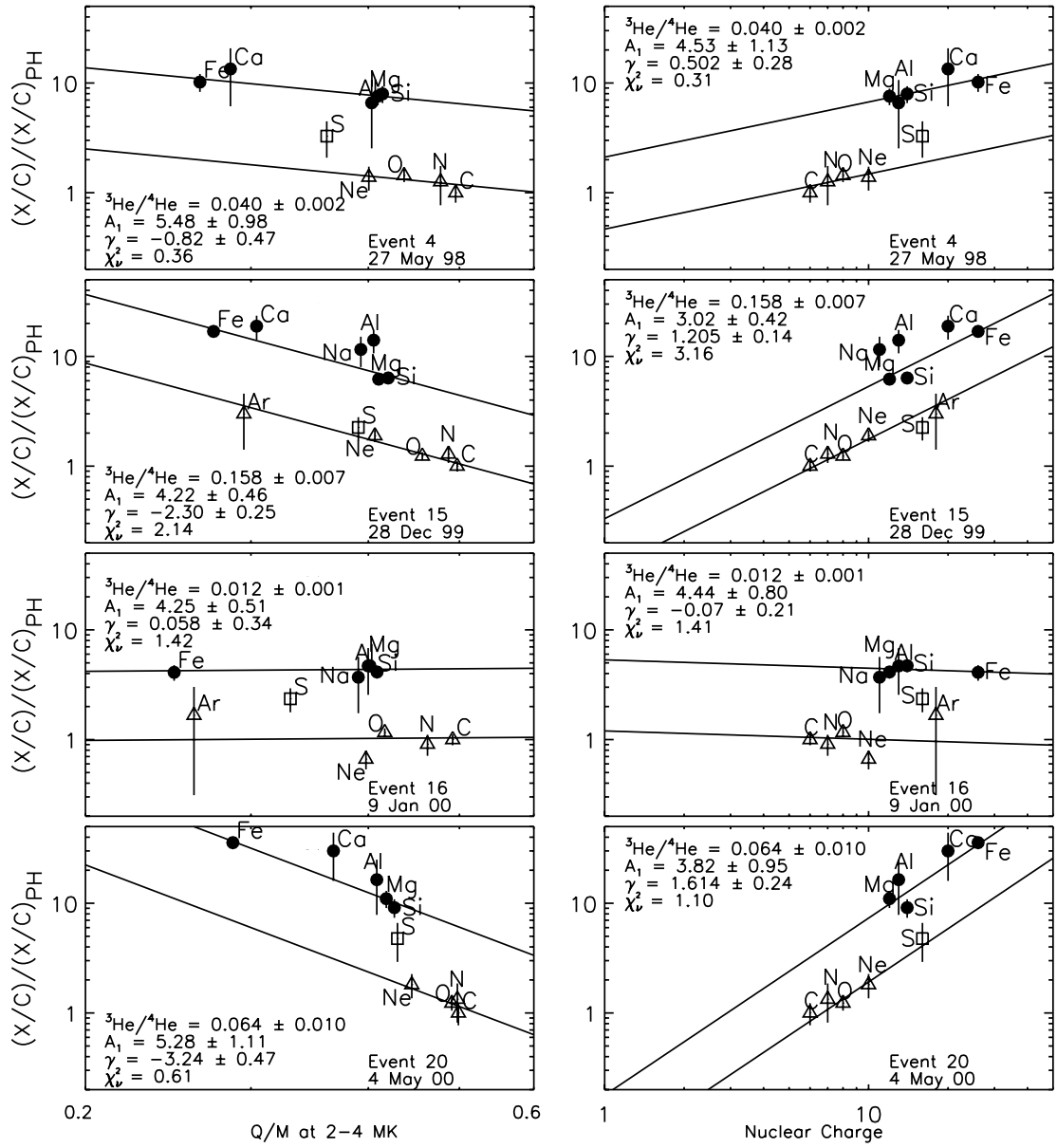

FIG. 5.—Heavy-element abundances with respect to C for four small SEP events, normalized to photospheric abundances (Grevesse & Sauval 1998), plotted against estimated Q/M at temperatures between 2 and 4 MK (*left panels*) and against nuclear charge Z (*right panels*). The uncertainty plotted for each data point include 1 standard deviation of statistical uncertainty on the SEP abundance of element X, and the uncertainty on X in the photosphere. Filled circles correspond to elements with FIP less than 10 eV, and open triangles to elements with FIP greater than 10 eV. The solid lines represent a fit with a power law times a step function in FIP, as described by eq. (2). The sulfur data point (FIP $\sim$ 10 eV), plotted as an open square, is not included in the fit.

The two lower panels in Figure 6 show the extracted FIP step magnitudes (A_1) from the fits with power laws in Q/M and in Z, plotted against the 0.5–2.0 MeV nucleon^{-1} ^{3}He/^{4}He ratios from ULEIS. In these plots the FIP factor is shown to be statistically significant and greater than 1 for almost every small SEP event in the study, including the ^{3}He-rich ones with heavy-element composition typical of impulsive SEP events. There also appears to be a great deal of variability in the FIP factor, as has already been shown in large SEP events (Garrard & Stone 1994; Mewaldt et al. 2000, 2002), with little dependence on the ^{3}He content. Finally, one can see that the FIP step magnitudes derived using a power law in Q/M with an assumed temperature spread of 2–4 MK (*left panel*) are better determined than those derived using a power law in Z (*right panel*). The other fits in Q/M with larger assumed temperature spreads (not shown) also yield better determinations of the FIP step magnitude than fits using a power law in Z.

For clarity, the lower two panels of Figure 6 have been further quantified in Figure 7. Figure 7 shows four histograms with the distributions of the sizes of the FIP steps, for the entire data set and for each of the three event subsets based on ^{3}He/^{4}He. Each histogram also contains a shaded region that corresponds to the weighted average of the FIP steps, with 1 standard deviation of uncertainty. This uncertainty is calculated by combining, in quadrature, the statistical uncertainties on the FIP steps with 1 standard deviation of the population spread in the histogram. The resulting uncertainties, shown in Figure 7, are dominated by the population spreads. From these four histograms it is clear that

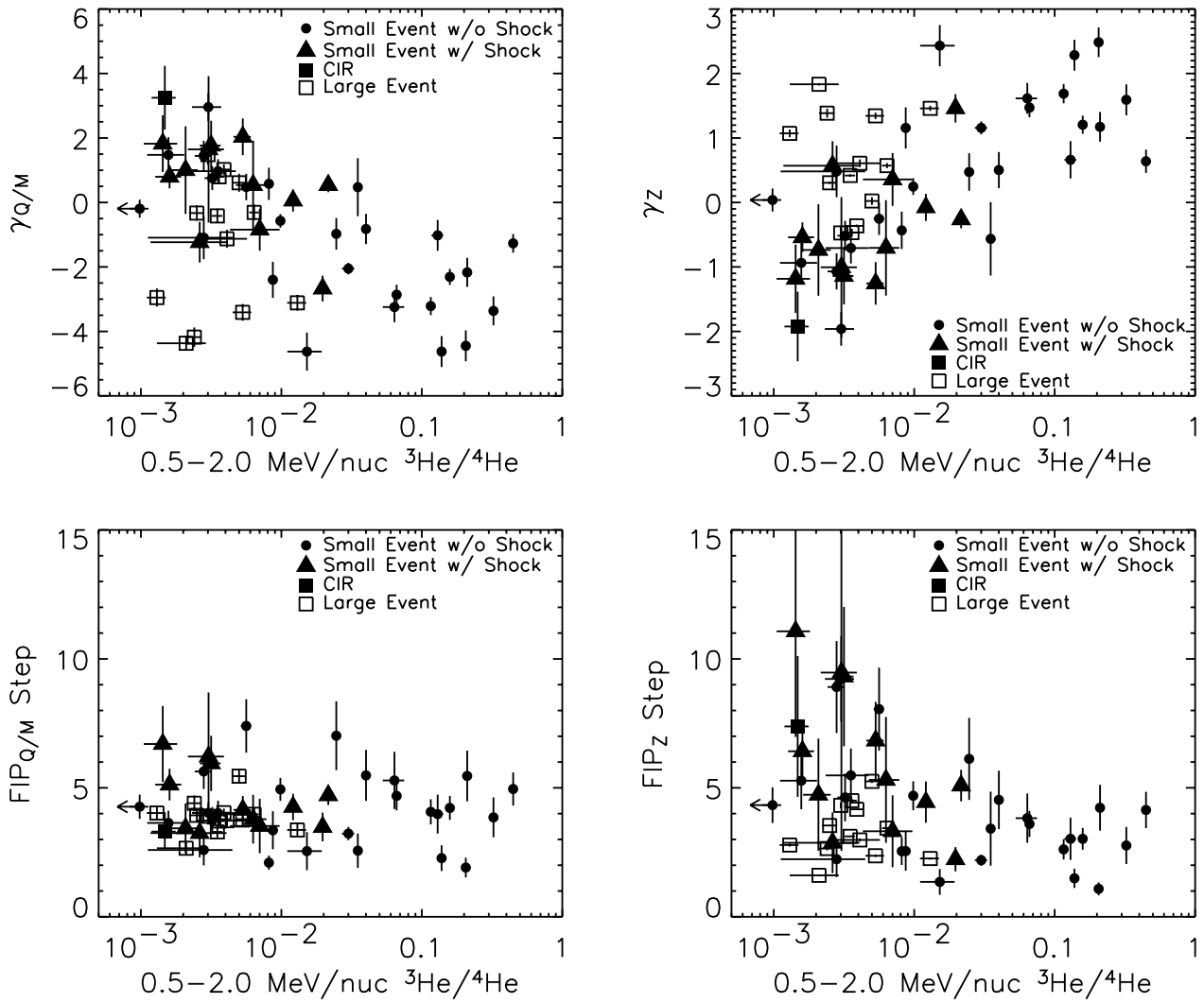

FIG. 6.—Two upper panels show plots of the Q/M (*left panel*) and Z (*right panel*) power-law indices with respect to the 0.5–2.0 MeV nucleon^{-1} ^{3}He/^{4}He ratios from ULEIS for the 39 small SEP events in this study (*filled symbols*), and for 13 large gradual SEP events (*open squares*). The lower panels depict the FIP steps derived from a fit with a power law in Q/M (*left panel*) and in Z (*right panel*) plotted against the 0.5–2.0 MeV nucleon^{-1} ^{3}He/^{4}He ratios from ULEIS. The charge states Q in the small SEP events are calculated as described in the text, assuming a temperature spread of 2–4 MK over the data set. The charge states in the 13 large SEP events are taken from Labrador et al. (2001).

the magnitude and variability of the FIP step are similar throughout the data set, within the stated uncertainties. Also of note is that the average FIP steps are consistent in magnitude with those measured in past studies of large gradual SEP events (4.3 ± 2.2 by Garrard & Stone 1994, and 3.9 ± 0.9 by Mewaldt et al. 2000, 2002). This similarity is not surprising, considering that the corona is known to be a source region in both gradual SEP events (Cook et al. 1984) and ^{3}He-rich events (Reames et al. 1994). However, the variability of the FIP steps derived from this data set ($\sim$2–7) is somewhat greater than the $\sim$3–7 found by Mewaldt et al. (2000, 2002) and the factor of 2 found by Garrard & Stone (1994) in large gradual events.

In order to check the reliability of the derived FIP values in the small SEP events, we have compared the values of the FIP step extracted from the fits using power laws in Q/M ($FIP_{Q/M}$), with varying temperature spreads and power laws in Z (FIP_Z). Figure 8 shows $FIP_{Q/M}$ at 2–4 MK plotted against $FIP_{Q/M}$ at 2–10 MK, and $FIP_{Q/M}$ at 2–4 MK plotted against FIP_Z, for the set of small SEP events. For reference, the dotted line in each panel represents a straight line through the origin with a slope of 1. From the left panel one can see that the derived FIP steps from power laws in Q/M are very consistent with one another and are not sensitive to the assumed range of charge states. It is also clear from the right panel that the FIP step derived from a power law in Z is reasonably consistent with that derived from Q/M, with possible differences for the larger FIP cases, although the uncertainties in FIP_Z are relatively large.

As a final check on the existence of a FIP step in the small SEP events, we have examined the effect of removing FIP from the model described by equation (2). Figure 9 shows the values of χ^2 per degree of freedom (χ^2_ν) from the fits using the function in equation (2) based on Q/M at 2–4 MK, plotted against (χ^2_ν) from the fits without a FIP step ($A_1 \equiv 1$ in eq. [2]). As evident in the figure, the removal of FIP from the model significantly increases the value of χ^2_ν and therefore worsens the quality of the fit to the data in each event. Figure 9 also shows that although the FIP model accounts for a significant part of the fractionation observed,

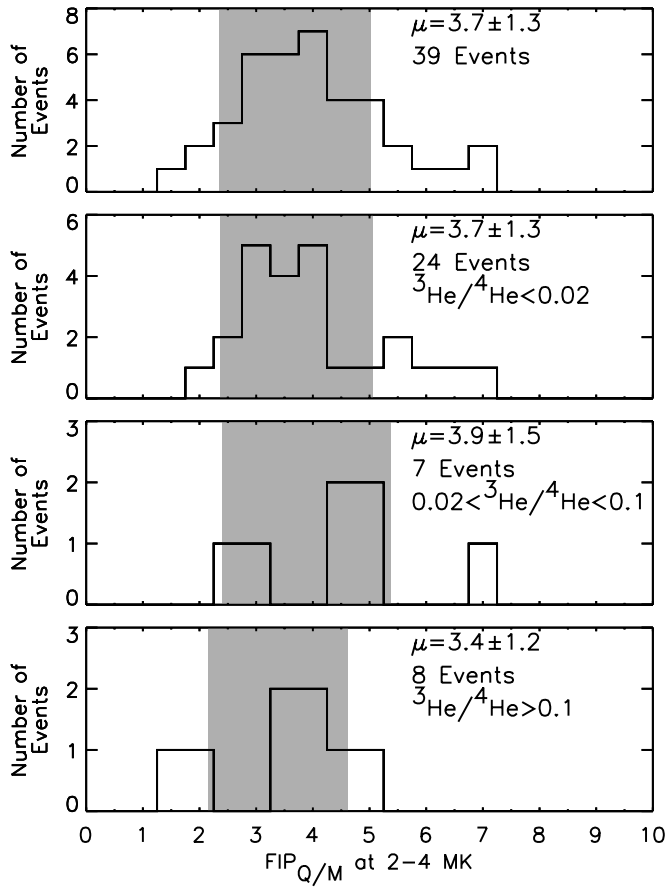

FIG. 7.—Histograms of the magnitudes of the derived FIP steps for all 39 events (*top panel*), the ^{3}He-poor events (*second panel*), moderately ^{3}He-rich events (*third panel*), and ^{3}He-rich events (*bottom panel*). The shaded regions denote the average values, calculated with a weighting factor of $1/\sigma^2$ on each FIP measurement. The averages are shown with 1 standard deviation of statistical uncertainty and population spread combined in quadrature.

many events have fits that result in a χ^2_ν value greater than 1 (e.g., Fig. 5, event 15). This indicates additional variability in the heavy-element abundances that is not accounted for by FIP or Q/M fractionation.

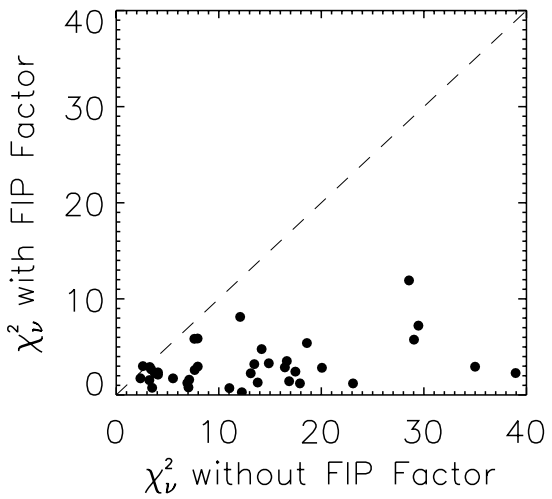

FIG. 9.—Values of χ^2 per degree of freedom (χ^2_ν) derived from fits to the small SEP event data with the functional form in eq. (2), plotted against the χ^2_ν values derived from fits with the functional form of a power law without a FIP step ($A_1 \equiv 1$ in eq. [2]). Both fits are performed under the assumption of a power law in Q/M with temperatures of 2–4 MK.

5. SUMMARY

The average 11–22 MeV heavy-element composition of the 39 small SEP events examined in this study was found to be in good agreement with that of past studies. The average composition of the eight ^{3}He-rich events agrees reasonably well with the previous study of 228 impulsive events by Reames et al. (1994), with the exception of Ne/C. The heavy-element abundances of the 24 events with $^3\mathrm{He}/^4\mathrm{He} < 0.02$ are strikingly consistent with coronal composition derived from large gradual SEP events.

In the 39 SEP events of this data set, there appears to be a trend toward increasing heavy-element content with increasing $^3\mathrm{He}/^4\mathrm{He}$ ratio. As noted by Dwyer et al. (2001), this behavior is likely due to mixing between impulsive SEP material and shock-accelerated coronal material and has been seen before in recent studies of small SEP events at lower energies (Ho et al. 2000; Dwyer et al. 2001).

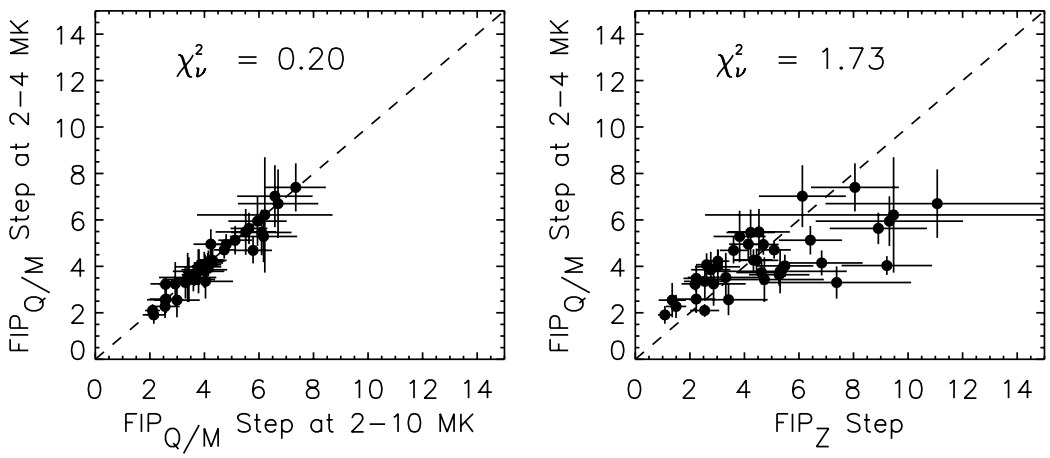

FIG. 8.—*Left panel*: FIP steps derived from a fit with a power law in Q/M with charge states indicative of equilibrium temperatures between 2 and 4 MK, plotted against the FIP steps derived from fits with temperatures between 2 and 10 MK. *Right panel*: Similar plot that compares the derived FIP steps from a fit with a power law in Q/M with temperatures between 2 and 4 MK, and the FIP steps derived from a fit with a power law in nuclear charge (Z). The dashed line in each panel is a straight line through the origin with a slope of 1.

The FIP effect has been measured in each of the small SEP events and has been found to vary in magnitude between approximately 2 and 7. This variability is somewhat greater than that found in previous studies of large gradual events. (Garrard & Stone 1994; Mewaldt et al. 2000, 2002). We do not find any dependence in the average size of the FIP factor on the ^{3}He content. This result is not unexpected, considering that the corona is known to be a source region in both gradual SEP events (Cook et al. 1984) and in ^{3}He-rich events (Reames et al. 1994). However, it is of note that the FIP factor in impulsive SEP event material, and therefore in impulsive SEP events, is consistent in magnitude but greater in variability than that found in previous studies of large gradual events (Garrard & Stone 1994; Mewaldt et al. 2000, 2002).

This research was supported by NASA at Caltech (under grant NAG5-6912), JPL, GSFC, The Aerospace Corporation (under NASA Cooperative Agreement 26979B), and the University of Maryland (under grant PC-251429). The authors thank R. E. Gold, D. K. Haggerty, and S. E. Hawkins for providing the electron and ion intensities, which were useful in this analysis. We thank C. W. Smith, H. Qiang, and R. M. Skoug for providing information about the interplanetary conditions relevant to this study. We are also grateful to H. V. Cane for helpful discussions related to this work.

APPENDIX

TABLE 4

11.0–21.8 MeV nucleon^{-1} Heavy-Element Intensities Relative to C

Event Number	C ÷ 1.00	N/C ÷ 2.51×10^{-1}	O/C ÷ 2.04	Ne/C ÷ 3.63×10^{-1}	Na/C ÷ 6.46×10^{-3}	Mg/C ÷ 1.15×10^{-1}	Al/C ÷ 8.91×10^{-3}	Si/C ÷ 1.07×10^{-1}	S/C ÷ 6.46×10^{-2}	Ar/C ÷ 7.59×10^{-3}	Ca/C ÷ 6.92×10^{-3}	Fe/C ÷ 9.55×10^{-2}
1	$4.09 \pm 0.37 \times 10^{-7}$	2.36 ± 0.33	1.58 ± 0.10	0.84 ± 0.14	3.92 ± 2.52	3.11 ± 0.37	1.69 ± 1.29	2.64 ± 0.37	0.81 ± 0.28	<1.66	<1.82	0.97 ± 0.34
2	$6.40 \pm 1.17 \times 10^{-7}$	0.84 ± 0.45	0.47 ± 0.13	0.56 ± 0.23	5.59 ± 4.41	1.97 ± 0.59	7.33 ± 4.96	2.38 ± 0.73	<0.91	<7.74	<8.49	6.19 ± 1.43
3	$1.08 \pm 0.20 \times 10^{-6}$	0.67 ± 0.39	0.49 ± 0.12	0.49 ± 0.22	<9.57	2.41 ± 0.70	2.23 ± 1.88	2.43 ± 0.77	1.62 ± 0.75	<8.14	<8.93	5.36 ± 1.35
4	$8.39 \pm 1.50 \times 10^{-7}$	1.26 ± 0.49	1.44 ± 0.17	1.39 ± 0.33	<9.25	7.58 ± 1.24	6.59 ± 4.03	7.96 ± 1.33	3.28 ± 1.14	<7.87	13.43 ± 7.29	10.19 ± 1.82
5	$1.13 \pm 0.11 \times 10^{-6}$	1.20 ± 0.24	1.00 ± 0.08	0.86 ± 0.15	3.94 ± 2.54	5.70 ± 0.59	5.73 ± 1.77	3.84 ± 0.51	2.50 ± 0.54	1.92 ± 1.59	3.48 ± 2.20	2.91 ± 0.55
6	$2.14 \pm 0.60 \times 10^{-7}$	1.17 ± 0.96	1.94 ± 0.33	4.54 ± 0.83	24.84 ± 14.96	17.12 ± 2.39	39.42 ± 12.94	15.34 ± 2.38	8.25 ± 2.51	10.17 ± 8.34	32.59 ± 14.92	34.48 ± 4.52
7	$1.17 \pm 0.14 \times 10^{-6}$	0.95 ± 0.26	0.97 ± 0.09	2.43 ± 0.28	8.23 ± 3.46	7.45 ± 0.75	9.08 ± 2.92	9.29 ± 0.94	6.54 ± 1.04	12.88 ± 4.42	14.30 ± 5.16	24.62 ± 1.89
8	$1.92 \pm 0.54 \times 10^{-7}$	<0.96	0.82 ± 0.30	0.67 ± 0.42	<16.70	5.42 ± 1.52	<12.10	3.63 ± 1.26	<1.67	<14.22	<15.59	<1.13
9	$2.32 \pm 0.18 \times 10^{-6}$	1.16 ± 0.18	0.75 ± 0.05	0.80 ± 0.11	2.61 ± 1.49	4.23 ± 0.39	5.14 ± 1.79	3.06 ± 0.37	1.32 ± 0.33	2.67 ± 1.41	6.92 ± 2.50	4.37 ± 0.55
10	$2.12 \pm 0.11 \times 10^{-6}$	1.51 ± 0.14	0.96 ± 0.04	1.11 ± 0.09	3.87 ± 1.25	4.86 ± 0.29	6.33 ± 1.35	4.79 ± 0.32	1.61 ± 0.24	0.90 ± 0.62	2.48 ± 1.03	3.71 ± 0.35
11	$6.75 \pm 0.55 \times 10^{-7}$	0.56 ± 0.20	0.61 ± 0.06	0.80 ± 0.12	<1.87	2.94 ± 0.35	1.32 ± 0.95	2.36 ± 0.34	1.22 ± 0.33	<1.59	4.39 ± 2.03	2.03 ± 0.40
12	$1.11 \pm 0.17 \times 10^{-6}$	1.03 ± 0.33	1.27 ± 0.13	0.95 ± 0.24	7.44 ± 5.55	3.00 ± 0.70	5.67 ± 3.35	6.26 ± 1.07	3.55 ± 1.05	<6.51	6.66 ± 4.89	7.99 ± 1.46
13	$2.57 \pm 0.55 \times 10^{-7}$	1.01 ± 0.47	1.23 ± 0.18	0.41 ± 0.24	<10.97	3.45 ± 0.80	<7.95	1.64 ± 0.61	1.20 ± 0.78	<9.34	<10.24	1.68 ± 0.92
14	$3.51 \pm 0.47 \times 10^{-7}$	0.39 ± 0.24	0.85 ± 0.10	1.24 ± 0.23	7.68 ± 3.92	7.16 ± 0.80	10.23 ± 3.65	6.07 ± 0.81	2.05 ± 0.66	<4.10	3.36 ± 2.94	5.20 ± 0.97
15	$1.67 \pm 0.15 \times 10^{-6}$	1.29 ± 0.21	1.23 ± 0.07	1.89 ± 0.20	11.56 ± 3.55	6.21 ± 0.58	14.06 ± 3.24	6.36 ± 0.61	2.25 ± 0.48	3.00 ± 1.57	18.87 ± 4.62	16.91 ± 1.22
16	$7.98 \pm 0.76 \times 10^{-7}$	0.91 ± 0.19	1.16 ± 0.07	0.66 ± 0.12	3.70 ± 1.96	4.13 ± 0.49	4.69 ± 2.11	4.71 ± 0.55	2.35 ± 0.52	1.66 ± 1.35	<2.54	4.10 ± 0.63
17	$6.89 \pm 1.15 \times 10^{-7}$	1.27 ± 0.36	0.45 ± 0.08	1.60 ± 0.33	8.43 ± 4.59	5.13 ± 0.94	1.87 ± 1.59	4.71 ± 0.95	2.69 ± 0.94	<7.19	18.42 ± 8.63	20.11 ± 2.44
18	$3.98 \pm 0.50 \times 10^{-7}$	1.07 ± 0.26	0.63 ± 0.07	0.32 ± 0.11	<4.88	2.07 ± 0.44	3.18 ± 2.17	1.43 ± 0.40	<0.49	<4.15	<4.55	<0.33
19	$1.82 \pm 0.28 \times 10^{-6}$	1.62 ± 0.34	1.65 ± 0.13	5.33 ± 0.54	26.52 ± 8.41	18.94 ± 1.66	28.04 ± 7.46	12.65 ± 1.49	1.98 ± 0.78	17.07 ± 6.59	23.80 ± 8.76	38.65 ± 3.12
20	$4.58 \pm 1.01 \times 10^{-7}$	1.34 ± 0.51	1.23 ± 0.16	1.81 ± 0.44	<14.54	11.01 ± 1.87	16.41 ± 8.48	9.12 ± 1.69	4.77 ± 1.77	<12.38	30.01 ± 14.00	35.70 ± 4.26
21	$1.58 \pm 0.14 \times 10^{-6}$	0.61 ± 0.13	0.92 ± 0.06	0.83 ± 0.13	5.16 ± 2.46	3.85 ± 0.45	2.00 ± 1.23	1.69 ± 0.32	0.58 ± 0.26	<2.39	<2.62	0.67 ± 0.29
22	$4.05 \pm 0.81 \times 10^{-7}$	0.67 ± 0.31	0.85 ± 0.13	0.76 ± 0.28	<12.11	3.63 ± 0.98	<8.78	1.70 ± 0.64	1.09 ± 0.74	<10.31	<11.31	<0.84
23	$1.60 \pm 0.41 \times 10^{-7}$	1.32 ± 0.57	1.98 ± 0.24	4.79 ± 0.83	<18.24	7.58 ± 1.53	<13.21	12.88 ± 2.27	9.55 ± 2.73	42.97 ± 17.03	19.87 ± 13.68	38.67 ± 5.05
24	$6.83 \pm 1.27 \times 10^{-7}$	0.48 ± 0.25	0.90 ± 0.12	1.36 ± 0.34	17.37 ± 9.37	7.11 ± 1.29	9.27 ± 4.82	6.93 ± 1.19	2.10 ± 0.90	<8.93	<9.79	11.05 ± 2.04
25	$2.51 \pm 0.14 \times 10^{-6}$	0.96 ± 0.10	0.83 ± 0.03	0.78 ± 0.08	4.37 ± 1.33	4.82 ± 0.32	5.01 ± 1.10	4.12 ± 0.30	1.28 ± 0.23	2.08 ± 0.91	9.55 ± 2.01	6.07 ± 0.46
26	$5.62 \pm 0.94 \times 10^{-7}$	0.67 ± 0.29	1.26 ± 0.13	2.52 ± 0.42	14.88 ± 7.54	5.60 ± 0.92	9.57 ± 4.99	6.93 ± 1.13	2.21 ± 0.97	10.91 ± 5.83	25.97 ± 10.23	14.98 ± 2.16
27	$8.55 \pm 0.85 \times 10^{-7}$	0.92 ± 0.19	1.17 ± 0.07	0.70 ± 0.13	6.59 ± 3.07	6.80 ± 0.64	5.48 ± 2.29	3.34 ± 0.49	0.36 ± 0.23	<2.73	<2.99	1.61 ± 0.47
28	$3.94 \pm 0.85 \times 10^{-7}$	1.66 ± 0.48	1.17 ± 0.16	0.56 ± 0.23	<16.91	4.68 ± 1.13	6.35 ± 4.04	2.84 ± 0.93	<1.69	<14.39	<15.78	<1.14
29	$5.73 \pm 1.14 \times 10^{-7}$	0.78 ± 0.32	1.46 ± 0.17	1.06 ± 0.32	9.18 ± 7.03	5.26 ± 1.15	4.85 ± 3.06	4.31 ± 1.14	3.09 ± 1.31	<11.53	34.92 ± 14.53	12.05 ± 2.41
30	$4.04 \pm 0.76 \times 10^{-7}$	0.81 ± 0.34	0.84 ± 0.12	0.56 ± 0.21	<11.54	5.59 ± 1.11	<8.36	4.25 ± 1.09	1.50 ± 0.81	<9.83	<10.77	1.69 ± 0.97
31	$7.28 \pm 0.67 \times 10^{-7}$	0.74 ± 0.16	0.67 ± 0.05	0.85 ± 0.14	3.67 ± 1.92	4.61 ± 0.52	4.30 ± 1.75	4.09 ± 0.53	1.49 ± 0.42	3.66 ± 1.91	11.57 ± 3.82	8.30 ± 0.90
32	$9.32 \pm 0.91 \times 10^{-7}$	0.93 ± 0.17	0.87 ± 0.06	0.50 ± 0.10	1.37 ± 0.59	3.81 ± 0.43	1.63 ± 0.95	2.39 ± 0.40	0.36 ± 0.25	<2.93	<3.22	0.88 ± 0.38
33	$3.57 \pm 0.54 \times 10^{-7}$	0.98 ± 0.29	0.83 ± 0.10	0.79 ± 0.21	7.33 ± 4.37	5.62 ± 0.81	<5.91	2.27 ± 0.63	<0.82	<6.95	<7.62	1.46 ± 0.80
34	$2.05 \pm 0.47 \times 10^{-7}$	1.26 ± 0.50	1.24 ± 0.18	0.40 ± 0.24	<15.15	3.99 ± 1.19	<10.97	5.90 ± 1.40	2.83 ± 1.40	<12.89	26.75 ± 13.28	34.48 ± 4.32
35	$5.19 \pm 0.44 \times 10^{-6}$	1.27 ± 0.17	1.05 ± 0.06	0.51 ± 0.09	2.61 ± 1.41	3.77 ± 0.41	4.19 ± 1.78	3.69 ± 0.48	0.84 ± 0.29	<2.18	3.24 ± 1.91	2.14 ± 0.44
36	$3.89 \pm 0.22 \times 10^{-6}$	0.80 ± 0.09	0.78 ± 0.03	0.29 ± 0.04	3.17 ± 1.11	2.65 ± 0.23	3.55 ± 0.95	1.97 ± 0.21	0.37 ± 0.13	<0.97	0.94 ± 0.73	0.36 ± 0.13
37	$3.09 \pm 0.58 \times 10^{-7}$	0.90 ± 0.35	1.08 ± 0.14	0.88 ± 0.28	11.88 ± 7.87	3.81 ± 0.94	3.51 ± 2.52	1.76 ± 0.67	<1.08	9.97 ± 6.03	<10.03	2.05 ± 1.05
38	$3.26 \pm 0.65 \times 10^{-7}$	<0.32	1.06 ± 0.14	1.95 ± 0.42	2.68 ± 1.62	5.15 ± 1.08	8.93 ± 5.46	6.13 ± 1.36	3.97 ± 1.39	18.09 ± 9.27	20.30 ± 10.71	29.00 ± 3.57
39	$2.27 \pm 0.10 \times 10^{-6}$	1.62 ± 0.11	0.83 ± 0.03	0.97 ± 0.07	2.94 ± 0.85	3.56 ± 0.22	4.79 ± 0.91	4.18 ± 0.25	1.17 ± 0.18	4.61 ± 1.08	7.95 ± 1.55	11.09 ± 0.51

Notes.—Table 4 is also available in machine-readable form in the electronic edition of the *Astrophysical Journal*. The table shows the 11.0–21.8 MeV nucleon^{-1} heavy-element intensities relative to C, divided by photospheric abundances (Grevesse & Sauval 1998) for the 39 SEP events in this study; 1 standard deviation of uncertainty is reported. The photospheric ratios used for the normalization are listed in the top row. The first column of the table denotes the event number. The C intensities are reported in units of particles (cm^2 sr s MeV nucleon^{-1})$^{-1}$, while all other abundances are given as dimensionless ratios. The uncertainties in each ratio $(X/C)/(X/C)_{PH}$ are statistical in nature and include only the uncertainty on X in the small SEP event.

REFERENCES

Breneman, H. H., & Stone, E. C. 1985, ApJ, 299, L57
Cohen, C. M. S., et al. 1999, Geophys. Res. Lett., 26, 2697
———. 2000, in AIP Conf. Proc. 528, Acceleration and Transport of Energetic Particles Observed in the Heliosphere, ed. R. A. Mewaldt et al. (Melville: AIP), 55
Cook, W. R., Stone, E. C., & Vogt, R. E. 1984, ApJ, 279, 827
Desai, M. I., Mason, G. M., Dwyer, J. R., Mazur, J. E., Smith, C. W., & Skoug, R. M. 2001, ApJ, 553, L89
Dwyer, J. R., Mason, G. M., Mazur, J. E., Gold, R. E., Krimigis, S. M., Moebius, E., & Popecki, M. 2001, ApJ, 563, 403
Fisk, L. A. 1978, ApJ, 224, 1048
Fisk, L. A., & Lee, M. A. 1980, ApJ, 237, 620
Fisk, L. A., et al. 1998, Space Sci. Rev., 83, 179
Garrard, T. L., & Stone, E. C. 1994, Adv. Space Res., 14, 589
Geiss, J. 1998, Space Sci. Rev., 85, 241
Geiss, J., et al. 1995, Science, 268, 1033
Gloeckler, G., & Geiss, J. 1998, Space Sci. Rev., 84, 275
Gold, R. E., et al. 1998, Space Sci. Rev., 86, 541
Gosling, J. T. 1993, J. Geophys. Res., 98, 18949
Grevesse, N., & Sauval, A. J. 1998, Space Sci. Rev., 85, 161
Ho, G. C., Roelof, E. C., Gold, R. E., Krimigis, S. M., Mason, G. M., Dwyer, J. R., & Mazur, J. E. 2000, in AIP Conf. Proc. 528, Acceleration and Transport of Energetic Particles Observed in the Heliosphere, ed. R. A. Mewaldt et al. (Melville: AIP), 99
Kahler, S. W. 1992, ARA&A, 30, 113
———. 1994, ApJ, 428, 837
Labrador, A. W., et al. 2001, Proc. 27th Int. Cosmic Ray Conf. (Hamburg), 3149
Leske, R. A., et al. 2001, Proc. 27th Int. Cosmic Ray Conf. (Hamburg), 3124
Mason, G. M., Mazur, J. E., & Dwyer, J. R. 1999a, ApJ, 525, L133
———. 2002a, ApJ, 565, L51
Mason, G. M., Reames, D. V., Klecker, B., Hovestadt, D., & von Rosenvinge, T. T. 1986, ApJ, 303, 849
Mason, G. M., et al. 1998, Space Sci. Rev., 86, 409
Mason, G. M., et al. 1999b, Space Sci. Rev., 89, 327
———. 2002b, ApJ, 574, 1039
Mazzotta, P., Mazzitelli, G., Colafrancesco, S., & Vittorio, N. 1998, A&AS, 133, 403
Mewaldt, R. A., et al. 2000, in AIP Conf. Proc. 528, Acceleration and Transport of Energetic Particles Observed in the Heliosphere, ed. R. A. Mewaldt et al. (Melville: AIP), 123
———. 2002, Adv. Space Res., 30, 79
Meyer, J.-P. 1985, ApJS, 57, 173
Miller, J. A. 1998, Space Sci. Rev., 86, 79
Moebius, E., et al. 2000, in AIP Conf. Proc. 528, Acceleration and Transport of Energetic Particles Observed in the Heliosphere, ed. R. A. Mewaldt et al. (Melville: AIP), 131
Reames, D. V. 1993, Proc. 23rd Int. Cosmic Ray Conf. (Calgary), 3, 388
———. 1995a, Rev. Geophys., 33, 585
———. 1995b, Adv. Space Res., 15, 741
———. 1998, Space Sci. Rev., 85, 327
———. 1999, Space Sci. Rev., 90, 413
Reames, D. V., Dennis, B. R., Stone, R. G., & Lin, R. P. 1988, ApJ, 327, 998
Reames, D. V., Meyer, J. P., & von Rosenvinge, T. T. 1994, ApJS, 90, 649
Reames, D. V., von Rosenvinge, T. T., & Lin, R. P. 1985, ApJ, 292, 716
Richardson, I. G., Reames, D. V., Wenzel, K.-P., & Rodriguez-Pacheco, J. 1990, ApJ, 363, L9
Slocum, P. L., et al. 2002, Adv. Space Res., 30, 97
Stone, E. C., et al. 1998, Space Sci. Rev., 86, 357
Temerin, M., & Roth, I. 1992, ApJ, 391, L105
Tylka, A. J., Cohen, C. M. S., Dietrich, W. F., Maclennan, C. G., McGuire, R. E., Ng, C. K., & Reames, D. V. 2001, ApJ, 558, L59
Widing, K. G., & Feldman, U. 1992, in Solar Wind Seven, ed. E. Marsch & R. Schwenn (Oxford: Pergamon), 405
———. 2001, ApJ, 555, 426
Wiedenbeck, M. E., et al. 2000, in AIP Conf. Proc. 528, Acceleration and Transport of Energetic Particles Observed in the Heliosphere, ed. R. A. Mewaldt et al. (Melville: AIP), 107